Data-Driven Tuning for Weighted Least Square of BLE-AoA-based Indoor Localization

Ginji Ohashi*, Shinsuke Ibi*, Takumi Takahashi†, and Hisato Iwai*
* Faculty of Science and Engineering, Doshisha University, 1-3 Tataramiyakodani, Kyotanabe, 610-0394, Japan
E-mail: ctwj0344@mail4.doshisha.ac.jp, {sibi, iwai}@mail.doshisha.ac.jp
† Graduate School of Engineering, Osaka University, Suita, Japan
E-mail: takahashi@comm.eng.osaka-u.ac.jp

***Abstract*—This paper proposes a novel positioning algorithm based on angle of arrival (AoA) in Bluetooth low energy (BLE), utilizing machine learning (ML) to achieve high-precision indoor positioning. Although various positioning methods use BLE, such as radio fingerprinting and proximity methods, the AoA method is known for its superior positioning accuracy and has received significant attention. However, similar to other methods, it is susceptible to the degradation of the positioning accuracy caused by the reflection, obstruction, and diffraction of radio waves by walls and furniture. To address this issue, we exploit ML techniques in the weighted least square (WLS) method in BLE-AoA systems. Using ML models trained on AoA datasets with supervised learning, the weights in the WLS method can be adjusted in a data-driven manner, thereby enhancing positioning accuracy. As the ML models, this paper utilizes weight learning model (WLM), random forest (RF), and multi-layer perceptron (MLP) and validates their effectiveness through computer simulations using publicly available datasets.**

I. Introduction

Indoor positioning, a technology for tracking and identifying the location of people or devices within indoor spaces, has seen an increasing demand over the past decade [1]. Its usage ranges widely from indoor navigation (in hospitals, office buildings, and airports) to object localization (in warehouses for goods and household items) [2]. Global navigation satellite system (GNSS) is a highly accurate and effective technology for use in outdoor environments. However, positioning accuracy is significantly degraded in indoor environments, where exterior walls create non-line-of-sight (NLOS) conditions [3]. Consequently, various indoor positioning technologies have been developed to replace GNSS, many of which utilize wireless technologies, such as ultra-wideband (UWB), Wi-Fi, and Bluetooth [4]. Among these technologies, Bluetooth low energy (BLE) is anticipated to play a crucial role in building wireless communication infrastructure for Internet of things (IoT) technologies owing to its low power consumption [5].

BLE offers multiple positioning metrics, each of which has its own advantages and disadvantages. Received signal strength indicator (RSSI) methods include proximity and fingerprinting; however, both achieve only meter-level accuracy, which is insufficient [6]. Additionally, methods such as time difference of arrival (TDoA) in GNSS or time of flight (TOF) in light detection and ranging (LiDAR) and ultrasonic sensors can lead to significant positioning errors owing to minor clock discrepancies between the transmitter and receiver, making them impractical for BLE, which assumes inexpensive devices [7]. However, BLE in Bluetooth 5.1 and beyond is equipped with direction-finding capabilities, enabling the acquisition of angle of arrival (AoA) using BLE devices [8]. Positioning methods using AoA can achieve centimeter-level accuracy; therefore, they are considered the most precise among BLE-based positioning methods and are attracting significant attention [9]. Therefore, this paper focuses on the AoA method for BLE. In the AoA method, two or more receivers with known positions receive direction-finding signals transmitted by a transmitter, and measure the AoA. The measured AoA is aggregated through the network into an upstream centralized system, where the estimated position coordinates of the transmitter are calculated.

Algorithms such as multiple signal classification (MUSIC) method calculate the AoA, and algorithms based on triangulation or the least square (LS) method calculate the estimated position coordinates [10]. Although the AoA method boasts high positioning accuracy, it is not immune to the effects of reflection, diffraction, and obstruction of radio waves by walls and furniture, which degrade positioning accuracy [11]. These radio propagation characteristics vary depending on the dimensions and layout of the indoor environment, which makes it challenging to address them using statistical methods. Therefore, many studies have explored the application of machine learning (ML) techniques to solve this issue. For example, [12] effectively addressed the AoA measurement error by integrating ML into the MUSIC algorithm.

In this study, we aim to enhance positioning accuracy by introducing ML into existing positioning algorithms. Specifically, we focus on the latest positioning algorithms based on the weighted LS (WLS) method [13], and propose a method to adjust the weights using ML models in a data-driven manner. As the ML models, this paper utilizes three ML models: weight learning model (WLM), random forest (RF), and multi-layer perceptron (MLP), to adjust the weights and evaluate each. The main contribution of this paper is to demonstrate the effectiveness of applying ML to the positioning algorithm of the BLE-AoA method through computer simulations using publicly available datasets created with commercially available BLE devices [14].

The remainder of this paper is organized as follows. Sect. II presents the system configuration and positioning algorithm

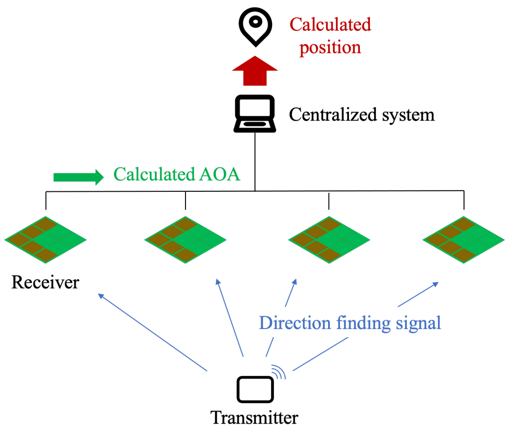

Fig. 1: Overview of AoA-Based positioning system.

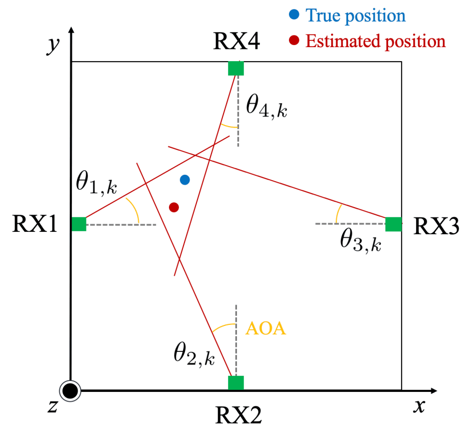

Fig. 2: AoA-Based estimation of transmitter position.

of the AoA-based positioning method. Sect. III explains the proposed machine-learning-based positioning algorithm. Sect. IV first describes the dataset and ML settings used for the simulations and then discusses the effectiveness of the proposed method based on the simulation results. Finally, Sect. V provides a summary and conclusion.

II. Indoor Positioning Using AoA

A. Positioning system configuration

Fig. 1 shows the configuration of the positioning system assumed in this paper. The transmitter, installed at an arbitrary location within the positioning environment, transmits direction-finding signals to the receivers fixed on walls and other surfaces. Each receiver calculates the AoA based on the received signal, and the calculated AoA is aggregated into a centralized system through the network. In the centralized system, the estimated position coordinates of the transmitter are calculated using positioning algorithms based on the triangulation method or LS method. In this study, we conducted offline simulations using a publicly available dataset that recorded the AoAs aggregated in a centralized system. Additionally, BLE allocates channels 37, 38, and 39 to transmit signals in the advertising channels. However, this paper only uses data from channel 37 to ignore the characteristic changes due to the different frequencies used.

B. Positioning algorithm

Fig. 2 is an overview of the AoA-based indoor positioning environment. The green squares represent the fixed receivers (RX1 to RX4), the blue plot represents the transmitter (TX). Let the total number of observed AoA data points be K, and the k-th AoA data point observed at the j-th RX be denoted by $\theta_{j,k}$ [degree]. In vector form, $\boldsymbol{\theta}_k = [\theta_{1,k}, \theta_{2,k}, \theta_{3,k}, \theta_{4,k}]$. The RX and TX position vectors are denoted as $\boldsymbol{a}_j = \left[x^{\mathrm{RX}j}, y^{\mathrm{RX}j}\right]^{\mathsf{T}} (j \in \{1,2,3,4\})$, $\boldsymbol{t}_k = \left[x_k^{\mathrm{TX}}, y_k^{\mathrm{TX}}\right]^{\mathsf{T}}$, respectively. The role of positioning is to estimate the position of TX $\hat{\boldsymbol{p}}_k = [\hat{x}_k, \hat{y}_k]^{\mathsf{T}}$ from observed AoA data $\boldsymbol{\theta}_k$, which is represented by red plot.

In the AoA method, the intersection of the AoAs is considered the estimated position coordinate. However, due to measurement errors in the AoAs, a single intersection point is rarely obtained, and only a candidate region for the estimated position coordinates is identified. Therefore, algorithms such as the LS method are used to determine the estimated position coordinates from the candidate region. In this algorithm, the estimated position vector is determined as the positions that minimize the sum of the squared perpendicular distances D_k from the red lines corresponding to $\boldsymbol{n}_{j,k}$, which is a unit direction vector given by

$$\boldsymbol{n}_{j,k} = \left[\cos\left(\frac{\theta_{j,k}}{180}\pi\right), \sin\left(\frac{\theta_{j,k}}{180}\pi\right)\right]^{\mathsf{T}}. \tag{1}$$

The distance D_k is expressed as

$$D_k = \sum_{j=1}^{4} (\boldsymbol{a}_j - \boldsymbol{p})^{\mathsf{T}} \left(\boldsymbol{I}_2 - \boldsymbol{n}_{j,k}\boldsymbol{n}_{j,k}^{\mathsf{T}}\right)(\boldsymbol{a}_j - \boldsymbol{p}), \tag{2}$$

where $\boldsymbol{p}$ is a position vector and $\boldsymbol{I}_2$ is the identity matrix with size of two. According to the LS approach, the position vector $\boldsymbol{p}$ that minimizes D_k, denoted as $\hat{\boldsymbol{p}}_k$, is defined as

$$\hat{\boldsymbol{p}}_k = \arg\min_{\boldsymbol{p}} D_k. \tag{3}$$

To find the optimal vector $\hat{\boldsymbol{p}}_k$, D_k is partially differentiated concerning $\boldsymbol{p}$, and the solution with the minimum value D_k is formulated as

$$\sum_{j=1}^{4} \left(\boldsymbol{I}_2 - \boldsymbol{n}_{j,k}\boldsymbol{n}_{j,k}^{\mathsf{T}}\right)(\boldsymbol{a}_j - \hat{\boldsymbol{p}}_k) = \boldsymbol{0}. \tag{4}$$

Denoting matrix and vector as

$$\boldsymbol{R}_k = \sum_{j=1}^{4} \left(\boldsymbol{I}_2 - \boldsymbol{n}_{j,k}\boldsymbol{n}_{j,k}^{\mathsf{T}}\right), \tag{5}$$

$$\boldsymbol{q}_k = \sum_{j=1}^{4} \left(\boldsymbol{I}_2 - \boldsymbol{n}_{j,k}\boldsymbol{n}_{j,k}^{\mathsf{T}}\right)\boldsymbol{a}_j, \tag{6}$$

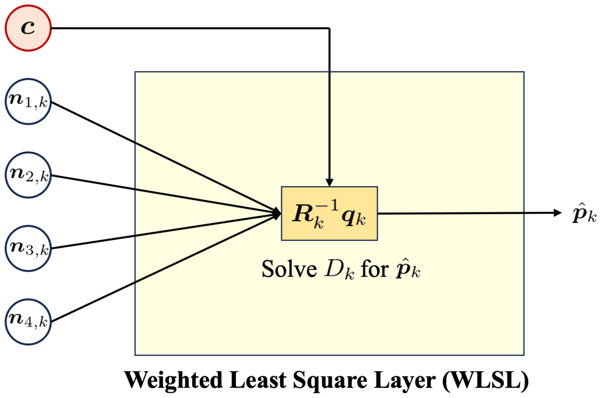

Fig. 3: Schematic of WLM-aided positioning algorithm.

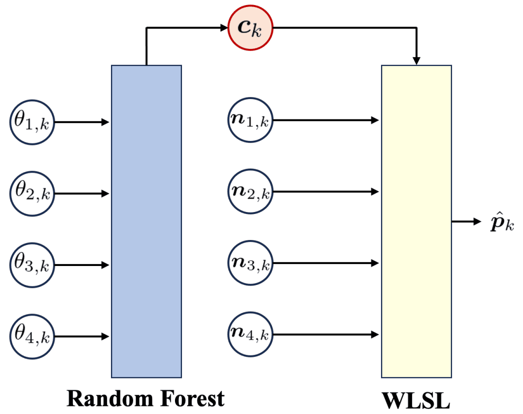

Fig. 4: Schematic of RF-aided positioning algorithm.

(4) is simply expressed as

$$\hat{\boldsymbol{p}}_k = \boldsymbol{R}_k^{-1}\boldsymbol{q}_k. \tag{7}$$

However, LS is vulnerable to uncertainties in the observed values and cannot minimize the mean square error (MSE), *i.e.*, the variance of the estimate [15].

WLS is an effective method to address this problem, and it utilizes

$$\boldsymbol{R}_k = \sum_{j=1}^{4} c_j \left(\boldsymbol{I}_2 - \boldsymbol{n}_{j,k}\boldsymbol{n}_{j,k}^{\mathsf{T}}\right), \tag{8}$$

$$\boldsymbol{q}_k = \sum_{j=1}^{4} c_j \left(\boldsymbol{I} - \boldsymbol{n}_{j,k}\boldsymbol{n}_{j,k}^{\mathsf{T}}\right)\boldsymbol{a}_j, \tag{9}$$

instead of (6). Here, $c_j \in [0, 1]$ is a weight coefficient for each AoA, and $c_j = 0$ means that RXj is not used in the calculation. Appropriately adjusting c_j can improve positioning accuracy; however, the adjustment method has not been sufficiently studied yet. If the statistical model of the observations is well-formulated, minimum MSE (MMSE) filtering should be applied. Otherwise, it is difficult to determine the optimal weight coefficients analytically. Therefore, this paper proposes a novel positioning algorithm that adjusts the weight c_j in a data-driven manner using ML models.

III. Machine Learning-Aided Positioning

A. Weight learning model

Fig. 3 is a schematic diagram of the positioning algorithm using WLM. In this algorithm, the weight vector $\boldsymbol{c} = [c_1, c_2, c_3, c_4]$ are trainable parameters, and the positioning accuracy is improved by using the optimal vectors obtained through the ML-based search. ML involves a training phase, during which the model is trained using training and validation data, and a test phase, during which the model is evaluated using test data. Yielding the unit direction vectors $\boldsymbol{n}_{j,k}$ into WLS layer (WLSL), the estimated position vector $\hat{\boldsymbol{p}}_k$ is calculated by (7) with the assistance of weight vector $\boldsymbol{c}$.

To adjust the weight $\boldsymbol{c}$, supervised learning is conducted in the training phase to minimize MSE loss function, which is expressed as

$$E = \frac{1}{K}\sum_{k=1}^{K} \|\hat{\boldsymbol{p}}_k - \boldsymbol{t}_k\|^2. \tag{10}$$

The gradient of $\boldsymbol{c}$ based on the error function is then calculated using the backpropagation method. The weights $\boldsymbol{c}$ are updated by an optimization algorithm using the obtained gradients. In the test phase, the weights are fixed to the optimized vectors obtained in the training phase.

B. Random forest

Fig. 4 shows a schematic diagram of the positioning algorithm using RF. The major difference of RF from the weight vector $\boldsymbol{c}$ of WLM is that the weight vector $\boldsymbol{c}_k = [c_{1,k}, c_{2,k}, c_{3,k}, c_{4,k}]$ can be adjusted for each data point k. RF is a ML model consisting of many decision trees. In this study, 100 decision trees are prepared. When $\boldsymbol{\theta}_k$ is yielded into the RF, each decision tree locally predicts weight vector, and the resultant output weight vector $\boldsymbol{c}_k$ of RF is selected by taking the majority vote of these local predictions.

Here, $c_j \in \{0, 1\}$ allowing the RF to classify whether each receiver is used ($c_j = 1$) or not ($c_j = 0$) for each $\boldsymbol{\theta}_k$. As c_j is a binary value, there are 16 $\left(2^4\right)$ candidates of weight vector $\boldsymbol{c}$. However, considering a constraint that at least two receivers are required for calculating the two-dimensional estimated position vector $\hat{\boldsymbol{p}}_k$, five cases where three or more $c_{j,k}$ are 0 are excluded, resulting in 11 candidate vectors: $\boldsymbol{c} \in \{[0,0,1,1], [0,1,0,1], [0,1,1,0], [0,1,1,1], [1,0,0,1], [1,0,1,0], [1,0,1,1], [1,1,0,0], [1,1,0,1], [1,1,1,0], [1,1,1,1]\}$.

For preparing labeled training data $\tilde{\boldsymbol{c}}_k$ of RF,

$$\tilde{\boldsymbol{c}}_k = \arg\min_{\boldsymbol{c}} \|\hat{\boldsymbol{p}}_k - \boldsymbol{t}_k\| \tag{11}$$

is found among 11 candidates, then dataset $(\boldsymbol{\theta}_k, \tilde{\boldsymbol{c}}_k)$ is provided into RF for supervised training.

In the training phase, the model parameters within RF are updated to ensure that the RF output vector $\boldsymbol{c}_k$ matches the labeled training data $\tilde{\boldsymbol{c}}_k$. In the test phase, the RF output vector

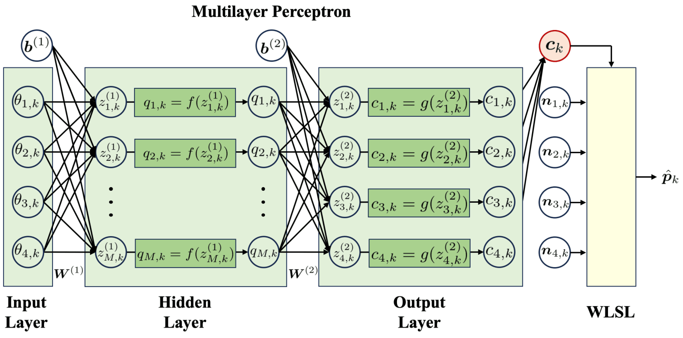

Fig. 5: Schematic of MLP-aided positioning algorithm.

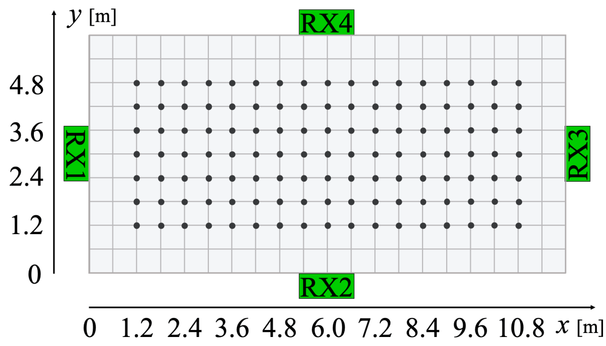

Fig. 6: Positioning environments.

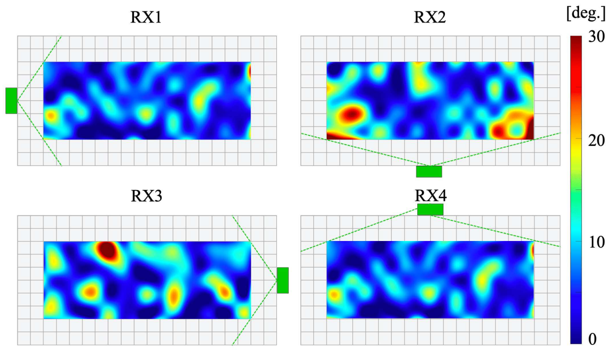

Fig. 7: Heatmaps of AoA measurement errors.

$\boldsymbol{c}_k$ obtained by yielding $\boldsymbol{\theta}_k$ into the trained RF and the unit direction vectors of the AoA $\boldsymbol{n}_{j,k}$ are provided into the WLSL for position estimation.

C. Multi-layer perceptron

Fig. 5 is a schematic diagram of the positioning algorithm using MLP. The MLP considered consists of an input layer, a hidden layer, and an output layer. Here, we define a weight matrix $\boldsymbol{W}^{(1)}$ of size $M \times 4$. The (j,m)-th element $w^{(1)}_{j,m}$ of $\boldsymbol{W}^{(1)}$ is the weight between the m-th node of the hidden layer and the j-th node of the input layer. Additionally, $\boldsymbol{b}^{(1)} = [b^{(1)}_1, \ldots, b^{(1)}_m, \ldots, b^{(1)}_M]^\mathsf{T}$ is a bias vector of size $M \times 1$. When $\boldsymbol{\theta}_k$ is yielded into the input layer, the input $z^{(1)}_{m,k}$ to the hidden layer is calculated as

$$z^{(1)}_{m,k} = \sum_{j=1}^{4} w^{(1)}_{m,j}\theta_{j,k} + b^{(1)}_m. \tag{12}$$

Thus, the input $\boldsymbol{z}^{(1)}_k = [z^{(1)}_{1,k}, \ldots, z^{(1)}_{m,k}, \ldots, z^{(1)}_{M,k}]^\mathsf{T}$ to the hidden layer is expressed as

$$\boldsymbol{z}^{(1)}_k = \boldsymbol{W}^{(1)}\boldsymbol{\theta}_k + \boldsymbol{b}^{(1)}. \tag{13}$$

$\boldsymbol{z}^{(1)}_k$ is then input to the activation function as

$$\boldsymbol{q}_k = f\left(\boldsymbol{z}^{(1)}_k\right) = \max\left(0, \boldsymbol{z}^{(1)}_k\right), \tag{14}$$

where the activation function $f(\cdot)$ of the hidden layer is the ReLU function.

In MLP, linear processing with weights and biases and nonlinear processing with activation functions are performed alternately, as described above. The input to the output layer is $\boldsymbol{z}^{(2)}_k = \boldsymbol{W}^{(2)}\boldsymbol{q}^{(1)}_k + \boldsymbol{b}^{(2)}$, where $\boldsymbol{W}^{(2)}$ and $\boldsymbol{b}^{(2)}$ are the weight matrix and bias vector between the hidden and the output layers, respectively. By using the sigmoid function as the activation function of the output layer $g(\cdot)$, the weights $\boldsymbol{c}_k$ are output as a vector with each component taking a value between 0 and 1 as

$$\boldsymbol{c}_k = g\left(\boldsymbol{z}^{(2)}_k\right) = \frac{1}{1 + \exp\left(-\boldsymbol{z}^{(2)}_k\right)}, \tag{15}$$

where the exponential function $\exp(\cdot)$ is extended to a vector-valued function. The obtained weights $\boldsymbol{c}_k$ and unit direction vectors of the AoA are input into the WLSL, and the estimated position coordinates $\hat{\boldsymbol{p}}_k$ are obtained.

In the training phase, similar to the explanation in Subsect. 3.A, the weights $\boldsymbol{W}^{(1)}, \boldsymbol{W}^{(2)}$ and biases $\boldsymbol{b}^{(1)}, \boldsymbol{b}^{(2)}$ between each layer of the MLP are updated iteratively to minimize the error function. In the test phase, positioning is performed by yielding $\boldsymbol{\theta}_k$ into the MLP, which has fixed weights and biases optimized in the training phase, and the obtained weights and unit direction vectors of the AoA into WLSL.

IV. Simulation Result

A. Simulation setup

This paper evaluates the proposed method using a publicly available dataset created in [14]. This dataset contains AoA data collected using four receivers (RX1 to RX4) and one transmitter (TX) in the room space of (12, 6, 3.1) meters, as shown in Fig. 6. To ignore the effects of human bodies, the transmitter and receivers were mounted on tripods and fixed at heights of 2.3 meters and 1.1 meters from the floor, respectively. In addition, the orientation of TX was fixed during the AoA measurements to eliminate the influence of its directionality and installation direction. The grid spacing on the floor was 60 cm, and the transmitter remained stationary for one minute at each of the 119 points indicated by black plots. The transmit power was set to 0 dBm, and the direction-finding signal transmission period was 50 Hz. However, due to packet loss, the AoA measured by the receivers is approximately 20

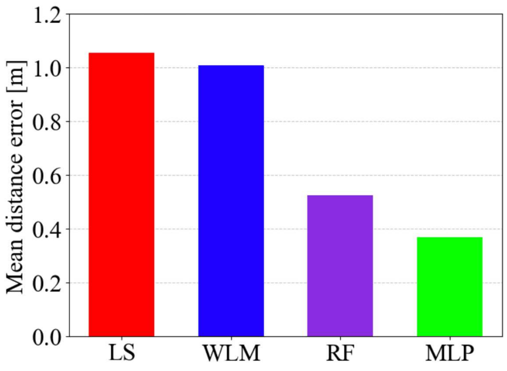

Fig. 8: MDE of estimated position coordinates.

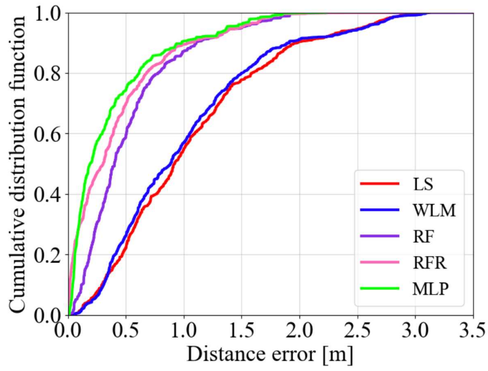

Fig. 9: CDF of DE in estimated position coordinates.

to 30 samples per second. As mentioned in Sect. II, this paper uses only data from channel 37 advertising channels; therefore, channel 37 data were extracted from the entire dataset. Furthermore, because the receivers were not time-synchronized during AoA measurements, temporal synchronization was performed on the post-measurement data by taking the median every second. Consequently, with $\boldsymbol{\theta}_k$ considered one sample, 60 samples were obtained per point, resulting in 7,140 samples across all data points (*i.e.*, $K = 7,140$). The entire dataset was randomly divided into training (50 %), validation (25 %), and test (25 %) data. The ML models were trained using the training and validation data, and then each method was evaluated using the test data.

Fig. 7 shows heatmaps of each receiver's mean absolute error (MAE) of the AoA. The MAE ranges from a minimum of approximately 0° to a maximum of approximately 60°, and positioning accuracy is expected to decrease in areas with high MAE. RX2 and RX4, installed along the long sides, show a common trend of increasing MAE as the distance from the center increases, whereas RX1 and RX3, installed along the short sides, do not show a common trend. This analysis suggests that the characteristics of the AoA cannot be predicted based on the installation positions of the receivers. The proposed method aims to improve positioning accuracy by adjusting the weights of the WLS method using a ML model trained on complex AoA characteristics. The following subsection discusses the evaluation results of the conventional and proposed methods using test data.

B. Evaluation using test data

The positioning accuracy of the conventional LS algorithm and the proposed methods using WLM, RF, and MLP is evaluated from the perspective of the distance error (DE) $|\hat{\boldsymbol{p}}_k - \boldsymbol{t}_k|$.

Fig. 8 shows the mean DE (MDE) for all 1,785 test data samples. The MDE of LS is 1.05 m, WLM is 1.01 m, RF is 0.52 m, and MLP is 0.37 m, indicating improved positioning accuracy for all proposed methods compared with conventional LS. MLP achieved about an approximately 65 % improvement in accuracy compared with the LS method. Moreover, the MDE follows the order of MLP <RF <WLM, indicating that RF is more accurate than WLM, and that MLP is more precise than RF. In the test phase, WLM has a lower degree of freedom in weight adjustment than the other two methods, as the weights are fixed over K samples. RF has a lower degree of freedom in weight adjustment than MLP because the possible values of each weight component are only 0 or 1. From this perspective, it is inferred that higher degrees of freedom in weight adjustment lead to improved positioning accuracy.

Fig. 9 shows cumulative distribution function (CDF) characteristics of DE for each method. While the BLE-AoA method is capable of centimeter-level positioning, only 55 % of the conventional LS methods resulted in less than 1 m DE. In comparison, 91 % of MLP and 87 % of RF have DE below 1 meter, demonstrating stable centimeter-level positioning. However, the maximum DE is about 2 to 3 m: 3.08 m for LS, 2.80 m for RF, and 2.23 m for MLP. Addressing these outliers remains a challenge for future works. On the other hand, in the figure, RFR represents a method using a Random Forest Regressor (RFR), where $c_{j,k}$ can take values of $\{0, 0.2, 0.4, 0.6, 0.8, 1.0\}$ as a simple extension of RF, increasing the number of weight candidates in RF to 1,225. As the number of weight candidates increases, improvements in CDF characteristics are observed, asymptotically approaching the performance of MLP. This result confirmed that, as mentioned earlier, the degree of freedom in weight adjustment is crucial for improving positioning accuracy. Furthermore, increasing the number of weight candidates in RF is expected to approach positioning accuracy comparable to MLP. However, as the number of weight candidates increases, the computational complexity required to label the training data increases exponentially, making MLP preferable considering the time cost.

Fig. 10 shows the DE heatmaps within the positioning area for LS and MLP. This figure demonstrates how the positioning accuracy improves at each point. While MLP shows an overall improvement in positioning accuracy, points with high DE in LS also have high DE in MLP. Similar trends were observed for WLM and RF. As ML learns the characteristics of the entire dataset, it may generalize poorly to data that deviate from the overall trend. Fig. 7 suggests that AoA measured in regions with significant positioning errors in LS likely has different

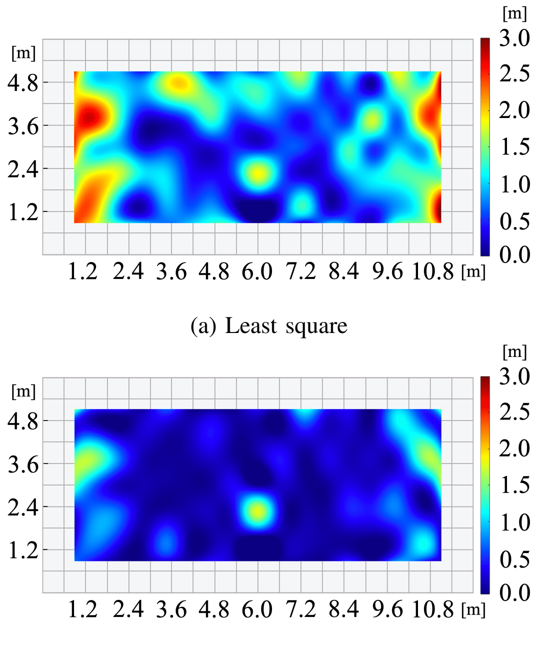

Fig. 10: Heatmaps of DE in estimated position coordinates.

characteristics from the other areas. The ML model might have generalized poorly to such data. Future studies should focus on generalizing the ML model to the entire area using various methods, such as increasing the number of datasets used for training and integrating the positioning results of multiple ML models.

V. Conclusions

In this paper, we proposed a positioning algorithm that uses ML to adjust the weights of the WLS method in a data-driven manner to improve the positioning accuracy of the BLE-AoA positioning method. Our research has significantly improved positioning accuracy across all three proposed methods. This confirms the effectiveness of integrating ML into the positioning algorithm. Additionally, it was found that the degree of freedom in weight adjustment is crucial for improving positioning accuracy. Acquiring generalization performance for the entire positioning area remains a challenge for the future.

Acknowledgment

A part of this work was financially supported by JSPS KAKENHI Grant Number JP23K20935, Japan.

References

[1] F. Zafari, A. Gkelias, and K. K. Leung, "A survey of indoor localization systems and technologies," *IEEE Communications Surveys & Tutorials*, vol. 21, no. 3, pp. 2568–2599, 2019.

[2] A. Koutris, T. Siozos, Y. Kopsinis, *et al.*, "Deep learning-based indoor localization using multi-view BLE signal," *Sensors*, vol. 22, no. 7, p. 2759, 2022.

[3] D. Dardari, P. Closas, and P. M. Djurić, "Indoor tracking: Theory, methods, and technologies," *IEEE Transactions on Vehicular Technology*, vol. 64, no. 4, pp. 1263–1278, 2015.

[4] H. Liu, H. Darabi, P. Banerjee, and J. Liu, "Survey of wireless indoor positioning techniques and systems," *IEEE Transactions on Systems, Man, and Cybernetics, Part C (Applications and Reviews)*, vol. 37, no. 6, pp. 1067–1080, 2007.

[5] C. Huang, Y. Zhuang, H. Liu, J. Li, and W. Wang, "A performance evaluation framework for direction finding using BLE AoA/AoD receivers," *IEEE Internet of Things Journal*, vol. 8, no. 5, pp. 3331–3345, 2021.

[6] L. Klinkusoom, T. Sanpechuda, K. Maneerat, K. Chinda, and L.-O. Kovavisaruch, "Accuracy comparison of Bluetooth Low Energy indoor positioning system based on measurement techniques," in *2022 IEEE International Conference on Consumer Electronics-Asia (ICCE-Asia)*, 2022, pp. 1–5.

[7] K. Zhao, T. Zhao, Z. Zheng, *et al.*, "Optimization of time synchronization and algorithms with TDOA based indoor positioning technique for Internet of Things," *Sensors*, vol. 20, no. 22, p. 6513, 2020.

[8] P. Mohaghegh, A. Boegli, and Y. Perriard, "Bluetooth Low Energy direction finding principle," in *2021 24th International Conference on Electrical Machines and Systems (ICEMS)*, 2021, pp. 830–834.

[9] Y. Zhuang, C. Zhang, J. Huai, Y. Li, L. Chen, and R. Chen, "Bluetooth localization technology: Principles, applications, and future trends," *IEEE Internet of Things Journal*, vol. 9, no. 23, pp. 23 506–23 524, 2022.

[10] G. Pau, F. Arena, Y. E. Gebremariam, and I. You, "Bluetooth 5.1: An analysis of direction finding capability for high-precision location services," *Sensors*, vol. 21, no. 11, p. 3589, 2021.

[11] A. Yassin, Y. Nasser, M. Awad, *et al.*, "Recent advances in indoor localization: A survey on theoretical approaches and applications," *IEEE Communications Surveys & Tutorials*, vol. 19, no. 2, pp. 1327–1346, 2017.

[12] A. Khan, S. Wang, and Z. Zhu, "Angle-of-Arrival estimation using an adaptive machine learning framework," *IEEE Communications Letters*, vol. 23, no. 2, pp. 294–297, 2019.

[13] N. Paulino and L. M. Pessoa, "Self-localization via circular Bluetooth 5.1 antenna array receiver," *IEEE Access*, vol. 11, pp. 365–395, 2023.

[14] M. Girolami, F. Furfari, P. Barsocchi, and F. Mavilia, "A Bluetooth 5.1 dataset based on Angle of Arrival and RSS for indoor localization," *IEEE Access*, vol. 11, pp. 81 763–81 776, 2023.

[15] S. O. Haykin, *Adaptive Filter Theory*, 5th. Hoboken: Pearson, 2013.